Supporting Information for

Hydrogen Activation and Metal Hydride formation Trigger Cluster Formation from Supported Iridium Complexes

Jing Lu, Ceren Aydin, Nigel D. Browning and Bruce C. Gates

Sample Synthesis and Handling

Zeolite- and MgO-supported mononuclear iridium complexes were prepared and handled with standard Schlenk line, glovebox, and glovebag techniques to exclude moisture and air. The precursor $Ir(C_2H_4)_2(acac)$ [acetylacetonatobis(ethene)-iridium(I)] was synthesized as described elsewhere.[1] Dealuminated zeolite HY (Zeolyst International, CBV760, Si:Al atomic ratio = 30), was calcined in O_2 at 773 K for 4 h and evacuated for 16 h at 773 K. MgO (EM Science, surface area 70 $m^2\ g^{-1}$) was mixed with deionized water to form a paste, which was dried overnight in air at 393 K. The resultant solid was ground and treated in O_2 as the temperature was ramped linearly from room temperature to 973 K and then held for 2 h. $Ir(C_2H_4)_2(acac)$ reacted at 298 K with the treated zeolite or MgO in a slurry in dried, deoxygenated *n*-pentane. The iridium content of each resultant powder was 1 wt%.

Sample handling for electron microscopy. To minimize the exposure to air and moisture, powder samples were loaded on a lacey carbon, 300-mesh copper grid (Ted-Pella) in the argon-filled glovebox. The grid was packed in an Eppendorf tube and sealed with Parafilm inside the glovebox. Each Eppendorf tube was placed into a stainless-steel Swagelok vacuum tube sealed with O-rings for transfer to the microscope. There, an argon-filled glovebag (Glas-Col) was purged 5 times with ultra-high-purity argon (Praxair, Grade 5.0), and the TEM grid was loaded onto the TEM holder under the blanket of flowing argon in the glovebag. The TEM holder was then inserted into the microscope with an air exposure less than 5 s.

Electron Microscope Imaging

Images were obtained with a JEOL JEM-2100F electron microscope at the University of California, Davis. The microscope was equipped with a FEG, operating at 200 kV, with a CEOS

hexapole probe (STEM) aberration corrector. The images were captured by an HAADF detector with a collection semi-angle of 75–200 mrad and a probe convergence semi-angle of 17.1 mrad. The imaging dose was ~10^5 e^- $Å^{-2}$. Prior to imaging of the sample, the aberration corrector was aligned with a Pt/Ir on holey carbon standard sample (SPI supplies) until atomic resolution of the metals was achieved and the lattice spacings of the metals in the standard sample were confirmed.

Infrared (IR) Spectroscopy

A Bruker IFS 66v/S spectrometer with a spectral resolution of 2 cm^{-1} was used to collect transmission IR spectra of powder samples. Approximately 30 mg of solid sample in the glove box was pressed into a thin wafer and loaded into a cell that served a flow reactor (In-situ Research Institute, Inc., South Bend, IN). The cell was sealed and connected to a flow system that allowed recording of spectra while the reactant gases flowed through the cell at a controlled temperature. Each spectrum is the average of 64 scans.

Isotopic H_2/D_2 Exchange Experiments.

Measurements of mass spectra were carried out to determine the products of the reaction in tubular plug-flow reactors identical to those used for the ethene hydrogenation measurements. The catalyst (20 mg) was diluted with 5 g of inert, nonporous α-Al_2O_3 and was loaded into the reactor in an inert-atmosphere glove box. The feed consisted of C_2H_4, H_2, and D_2 (the partial pressure of each was 200 mbar balanced in helium) with the total flow rate being 100 mL(NTP)/min and the total pressure being atmospheric. The temperature was 298 ± 1 K, controlled with a cooling jacket filled with water. Mass spectra of the gases introduced into the flow system and the effluents produced by reaction were measured with an online Balzers OmniStar mass spectrometer running in multi-ion monitoring mode. Specifically, changes in the signal intensities of H_2 (*m/z* = 2), D_2 (*m/z* = 4), HD (*m/z* = 3), CO (*m/z* = 28), C_2H_4 (*m/z* = 26, 27, and 28), C_2H_6 (*m/z* = 26, 27, 28, and 30), C_4H_8 (*m/z* = 41 and 55), and C_4H_{10} (*m/z* = 43 and 56) were recorded. The reported intensity values were corrected by subtracting background intensities recorded while the reaction gas mixture was bypassing the flow reactor containing the catalyst. The HD exchange was measured at room temperature for times on stream <10 min, for which the nuclearity of the iridium complexes initially present as single-atom complexes was

maintained, as demonstrated by EXAFS spectroscopy. The error bound, correspond to the standard deviation of the measurements, is estimated to be ± 1%

X-Ray Absorption Spectroscopy (XAS) Data Collection

The X-ray absorption spectra were recorded at beam line 10-ID (MR-CAT) at Argonne National Laboratory and Stanford Synchrotron Radiation Lighsource. A Si (111) or Si (220) double-crystal monochromator was used, which was detuned to 80% of maximum intensity to reduce the interference of higher harmonics present in the X-ray beam.

The mass of the sample (approximately 0.25 g) was chosen to give an absorbance between 1.5 and 3.0 calculated at 50 eV above the Ir L_{III} edge (11215 eV). The powder sample was loaded into a cell that served as a flow reactor.[2] X-ray intensity data were collected in transmission mode by use of ion chambers mounted on each end of the sample cell. For calibration purposes, measurement of the absorption of a platinum foil, placed after the sample, was carried out simultaneously.

Extended X-Ray Absorption Fine Structure (EXAFS) Data Analysis

Analysis of the EXAFS data was carried out with the software ATHENA of the IFEFFIT[3,4] package and with the software XDAP developed by Vaarkamp et al.[5] Each spectrum that was subjected to analysis was the average of four spectra. Details of the data processing and analysis methodology are reported elsewhere.[6,7]

The error in the data was calculated as the root mean square of the value obtained from the subtraction of smoothed χ data from the background-subtracted experimental χ values. Goodness of fit values was calculated with the software XDAP[5] as follows:

$$goodness\ of\ \ fit = \frac{\nu}{NPTS\left(\nu - N_{\text{free}}\right)} \sum_{i=1}^{NPTS} \left(\frac{\chi_{\text{exp},i} - \chi_{\text{model},i}}{\sigma_{\text{exp},i}} \right)^2$$

Where the terms χ_{model} and χ_{exp} are the model and experimental EXAFS values, respectively; σ_{exp} is the error in the experimental results; ν is the number of independent data points in the fit range; and NPTS is the actual number of data points in the fit range; *N* is the number of free parameters.

In the development of best-fit models of each of EXAFS data set, various combinations of plausible absorber–backscatterer contributions were fitted initially, which led to a list of candidate models narrowed on the basis of the goodness of fit and the overall fit in both *k* space and in *R* space. Then, a "difference-file" technique was applied to the candidate models, whereby the calculated EXAFS contribution from each individual Ir–backscatterer contribution was compared with the data in *R* space (calculated by subtracting all the other calculated Ir–backscatterer contributions from the experimental overall contributions). This iterative fitting was continued in *R* space for both overall and individual contributions with the Fourier-transformed EXAFS (χ) data until the best-fit model was obtained, which is the one providing optimum agreement between the calculated k^0-, k^1-, k^2-, and k^3-weighted EXAFS data and the model.

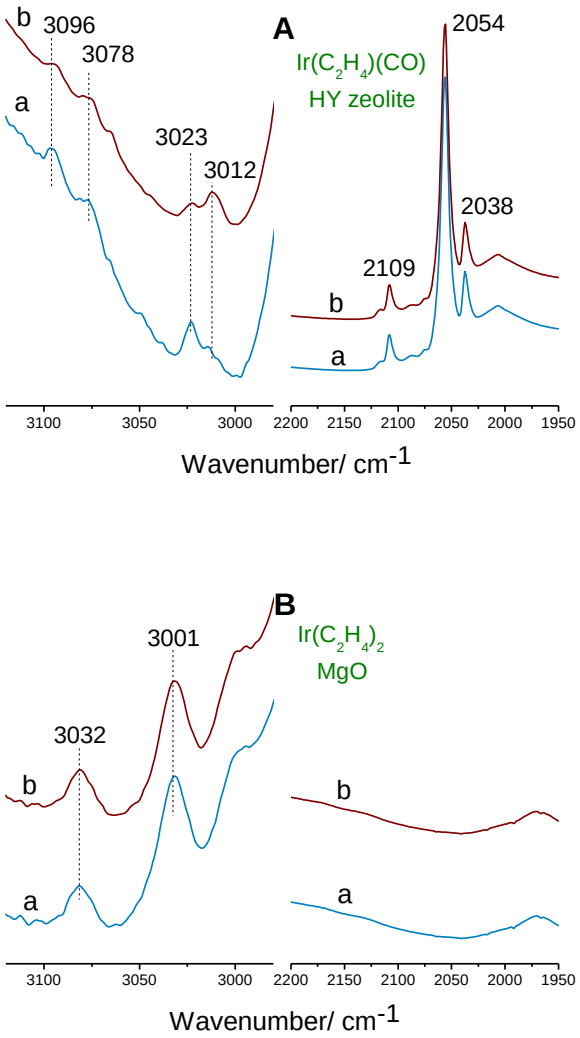

Figure S1. IR spectra (absorbance) in the ν_{CH} region (left) and ν_H/ν_{CO} region (right) characterizing $Ir(C_2H_4)(CO)$ on HY zeolite (A) and $Ir(C_2H_4)_2$ on MgO (B) in: (a) flowing helium and (b) flowing H_2 for 30 min at room temperature and 1 bar. The data indicate that the π-bonded ethene ligands are highly stable in flowing H_2 for these two iridium complexes, and there is no evidence of hydride formation.

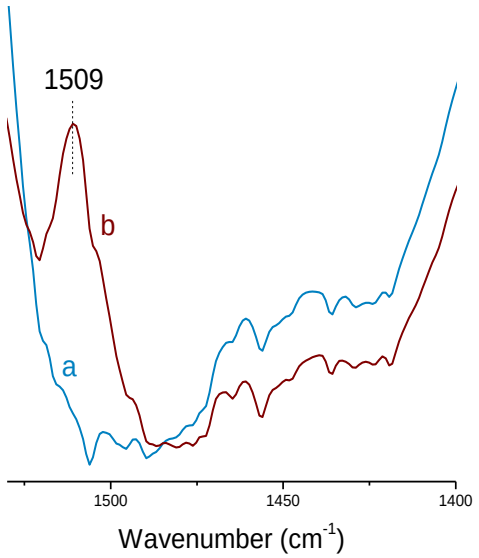

Figure S2. IR spectra characterizing zeolite Y-supported $Ir(C_2H_4)_2$ species under the following conditions: a) helium flowing at 300 K and 1 bar, and b) D_2 flowing at 300 K and 1 bar.

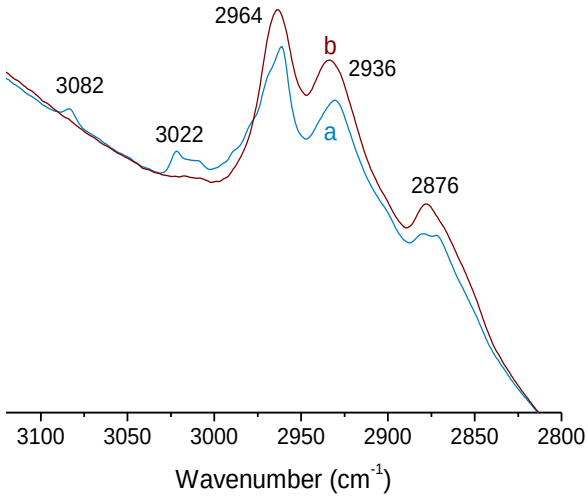

Figure S3. IR spectra in the ν_{CH} region characterizing Y zeolite-supported $Ir(C_2H_4)_2$ treated in flowing H_2 at 300 K for the following times (min): (a) 0 (blue line), (b) 10 (red line).

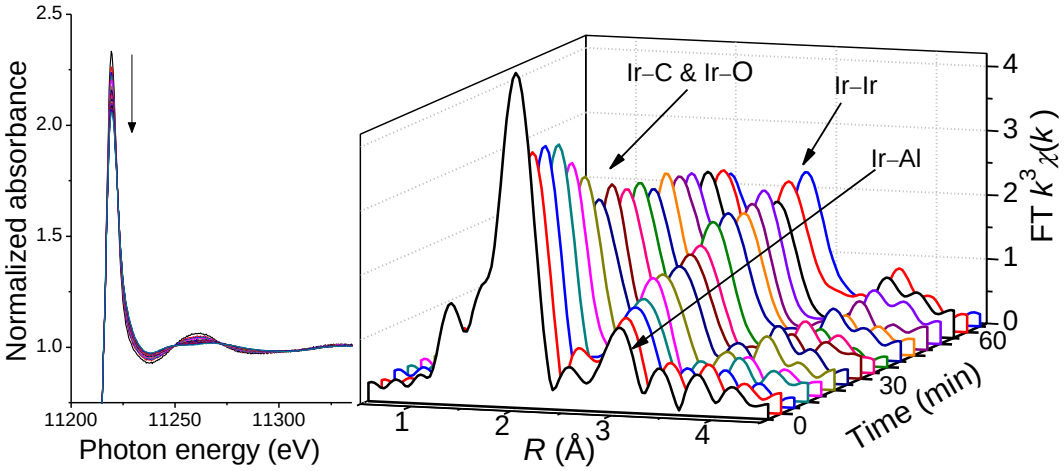

Figure S4. XANES spectra (left) and the phase-corrected Fourier transform (FT) function determined from transient EXAFS spectra (right) characterizing samples initially incorporating $Ir(C_2H_4)_2$ on HY zeolite in flowing H_2 at 300 K and 1 bar for 1 h.

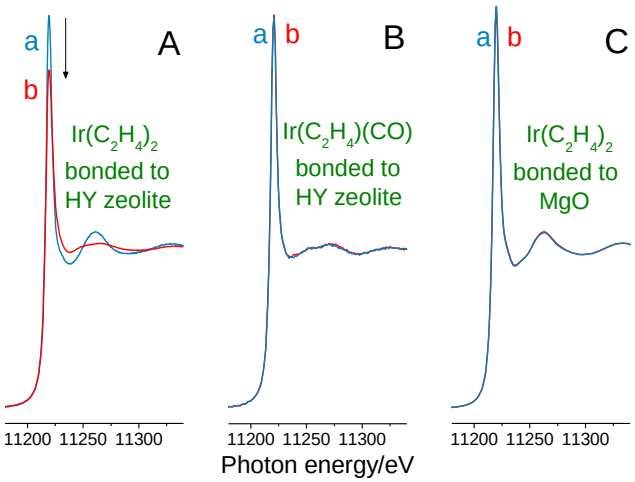

Figure S5. XANES spectra at the Ir L_{III} edge characterizing samples initially consisting of (A) $Ir(C_2H_4)_2$ on HY zeolite, (B) $Ir(C_2H_4)(CO)$ on HY zeolite, and (C) $Ir(C_2H_4)_2$ on MgO treated in (a) flowing helium and (b) flowing H_2 at 300 K and 1 bar for 1 h.

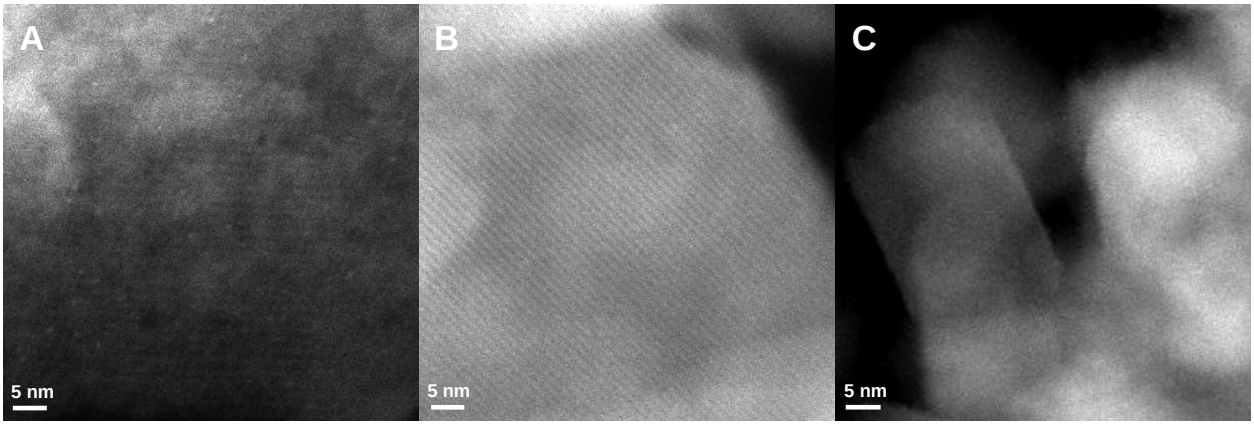

Figure S6. Aberration-corrected HAADF-STEM (Z–contrast) images characterizing initially prepared $Ir(C_2H_4)_2$ on HY zeolite (A), $Ir(C_2H_4)(CO)$ on HY zeolite (B), and $Ir(C_2H_4)_2$ on MgO (C) after treatment in flowing H_2 at 300 K for 1 h. The images were recorded at lower magnifications than those shown in Figure 4 in the text.

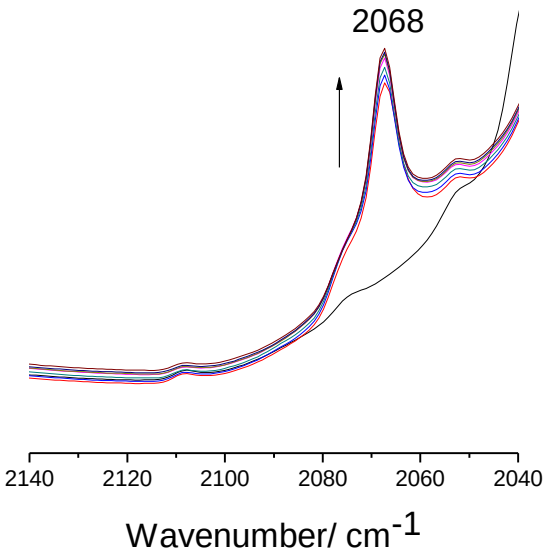

Figure S7. IR spectra (absorbance) in the ν_H region (right) characterizing HY-zeolite supported $Ir(C_2H_4)_2$ in flowing H_2 at 300 K and 1 bar for 1 h. The position of the band at 2068 cm^{-1} is stable but its intensity increased, indicating that clusters formed by reaction with H_2 and incorporate Ir–H species.

Table S1. Summary of structural parameters corresponding to the fit models characterizing EXAFS data representing the supported iridium species (at room temperature and 1 bar).

Model	Absorber – backscatter pair	*N*	*R*(Å)	$10^3 \times \Delta\sigma^2$ (Å^2)	ΔE_0 (eV)	*k* range	*R* range	Error in EXAFS function	Goodness of fit
$Ir(C_2H_4)_2$ on zeolite HY in helium	Ir-$O_{zeolite}$	2.0	2.10	0.6	-5.9	3.79 – 13.01	0.5 – 3.5	0.0009	2.9
	Ir-C	4.1	2.03	9.0	0.26				
	Ir-Al	1.0	2.97	8.8	-8.0				
	Ir-Ir	[b]	[b]	[b]	[b]				
$Ir(C_2H_4)_2$ on zeolite HY after being in H_2 for 15 min	Ir-$O_{zeolite}$	1.2	2.12	12	-8.0	3.82 – 12.53	0.5 – 3.5	0.0009	1.4
	Ir-C	2.0	2.05	9.5	-1.5				
	Ir-Al	0.7	2.99	6.6	-8.0				
	Ir-C_{long}	1.8	3.06	11	3.7				
	Ir-Ir	[b]	[b]	[b]	[b]				
$Ir(C_2H_4)_2$ on zeolite HY after being in H_2 for 1 h	Ir-$O_{zeolite}$	0.7	2.14	7.4	-7.9	4.03 – 12.66	0.5 – 3.5	0.0009	2.2
	Ir-C	1.1	2.05	12	-2.4				
	Ir-Al	0.5	3.01	1.2	-7.2				
	Ir-Ir	1.3	2.67	6.4	1.8				
$Ir(C_2H_4)(CO)$ on zeolite HY in helium[a]	Ir-$O_{zeolite}$ & Ir-C	3.6	2.13	8.8	-8.0	3.98 – 13.38	0.5 – 3.5	0.0007	14
	Ir-C_{co}	1.3	1.85	9.3	2.0				
	Ir-O_{co}	1.3	2.97	14	-6.3				
	Ir-Al	1.1	3.01	5.6	-8.0				
	Ir-Ir	[b]	[b]	[b]	[b]				
$Ir(C_2H_4)(CO)$ on zeolite HY after being in H_2 for 1 h	Ir-$O_{zeolite}$ & Ir-C	3.5	2.13	9.6	-5.5	3.98 – 13.01	0.5 – 3.5	0.0007	9.8
	Ir-C_{co}	1.4	1.88	11	1.6				
	Ir-O_{co}	1.4	2.91	13	-5.4				
	Ir-Al	1.1	2.99	4.8	-2.7				
	Ir-Ir	[b]	[b]	[b]	[b]				
$Ir(C_2H_4)_2$ on MgO in helium[a]	Ir-O_{MgO}	2.1	2.01	5.8	-7.4	3.88 – 13.44	0.5 – 3.5	0.0004	12
	Ir-C	4.1	2.13	6.0	-6.2				
	Ir-Mg	1.5	3.06	9.4	-5.0				
	Ir-Ir	[b]	[b]	[b]	[b]				
$Ir(C_2H_4)_2$ on MgO after being in H_2 for 1 h	Ir-O_{MgO}	1.9	2.06	3.9	-3.4	3.81 – 13.15	0.5 – 3.5	0.0004	14
	Ir-C	3.8	2.12	6.1	-7.0				
	Ir-Mg	1.6	2.98	11	0.8				
	Ir-Ir	[b]	[b]	[b]	[b]				

[a] values obtained from ref. 20 in the text. [b] Contribution not detectable. [c] Fit details: $0.5 < R < 3.2$ Å, $3.84 < k < 12.06$ Å^{-1}, error: 0.0006, goodness of fit: 5.7. [d] Notation: *N*, coordination number; *R*, distance between absorber and backscatterer atoms; $\Delta\sigma^2$, disorder term sometimes called Debye-Waller factor; ΔE_0, inner potential correction. Error bounds (accuracies) characterizing the structural parameters obtained by EXAFS spectroscopy are estimated to be as follows: *N*, ±20%; *R*, ±0.02Å; $\Delta\sigma^2$, ±20%; and ΔE_0, ±20%. [e] The number of statistically justified parameters was calculated according to the Nyquist theorem as follows: number of justified parameters $n = (2\Delta k \Delta R/\pi) + 2$, where Δk and ΔR are the *k*- and *R*-ranges used for the fitting, respectively.

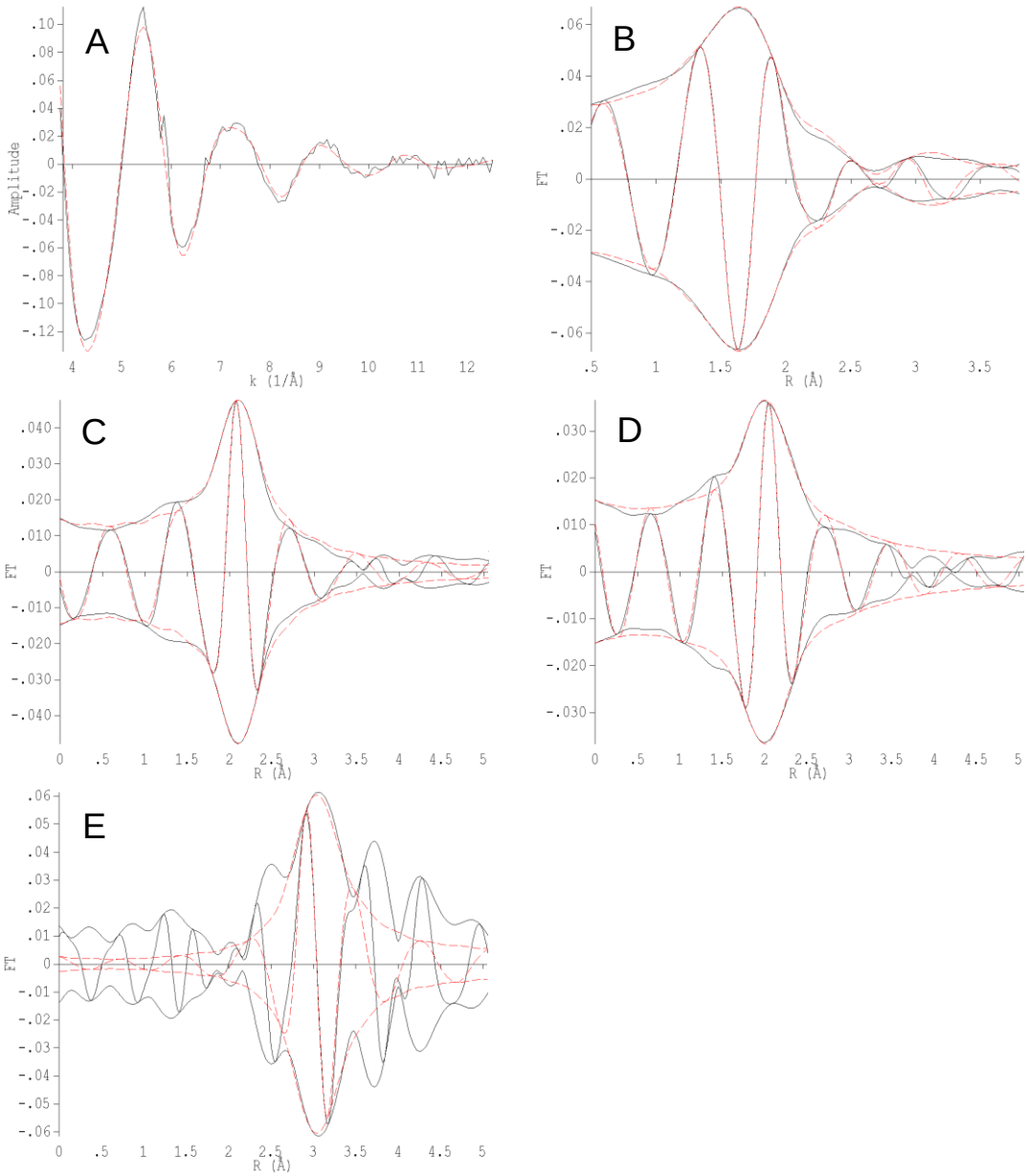

Figure S8. EXAFS data characterizing zeolite HY-supported $Ir(C_2H_4)_2$ in flowing helium at 300 K: (A) k^1-weighted EXAFS function, $k^1(\chi)$ (solid line) and sum of the calculated contributions (dashed line); (B) k^1-weighted imaginary part and magnitude of the Fourier transform of the data (solid line) and sum of the calculated contributions (dashed line); (C) k^1-weighted, phase-corrected, imaginary part and magnitude of the Fourier transform of the data (solid line) and calculated contributions (dashed line) of the $Ir–O_{zeolite}$ shell; (D) k^1-weighted, phase-corrected, imaginary part and magnitude of the Fourier transform of the data (solid line) and calculated contributions (dashed line) of the Ir–C shell; (E) k^2-weighted, phase-corrected, imaginary part and magnitude of the Fourier transform of the data (solid line) and calculated contributions (dashed line) of the Ir–Al shell.

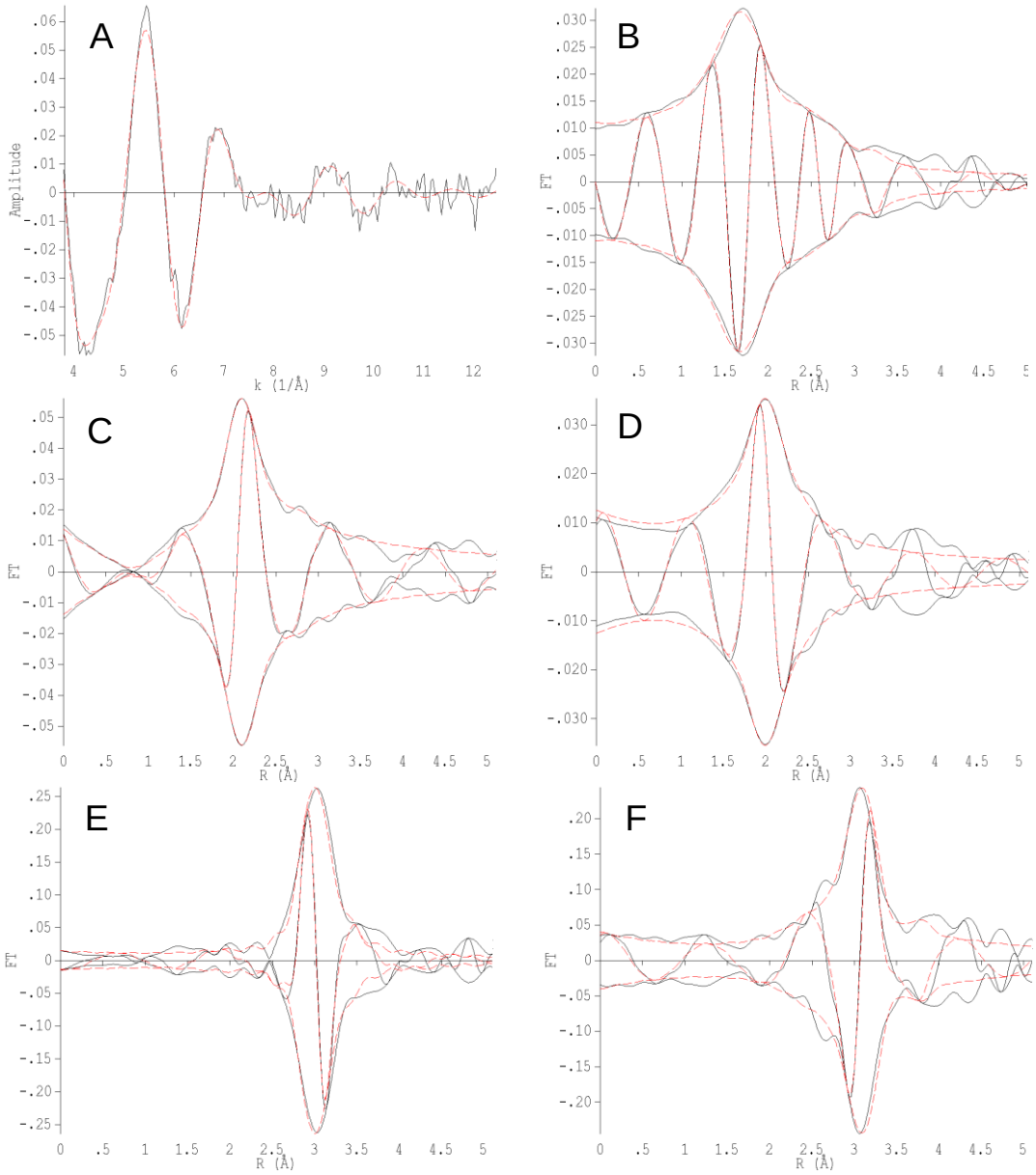

Figure S9. EXAFS data characterizing zeolite HY-supported $Ir(C_2H_4)_2$ after treatment in flowing H_2 at 300 K for 15 min: (A) k^1-weighted EXAFS function, $k^1(\chi)$ (solid line) and sum of the calculated contributions (dashed line); (B) k^1-weighted imaginary part and magnitude of the Fourier transform of the data (solid line) and sum of the calculated contributions (dashed line); (C) k^1-weighted, phase-corrected, imaginary part and magnitude of the Fourier transform of the data (solid line) and calculated contributions (dashed line) of the Ir–$O_{zeolite}$ shell; (D) k^1-weighted, phase-corrected, imaginary part and magnitude of the Fourier transform of the data (solid line) and calculated contributions (dashed line) of the Ir–C shell; (E) k^2-weighted, phase-corrected, imaginary part and magnitude of the Fourier transform of the data (solid line) and calculated contributions (dashed line) of the Ir–C_{long} shell; (F) k^2-weighted, phase-corrected, imaginary part and magnitude of the Fourier transform of the data (solid line) and calculated contributions (dashed line) of the Ir–Al shell.

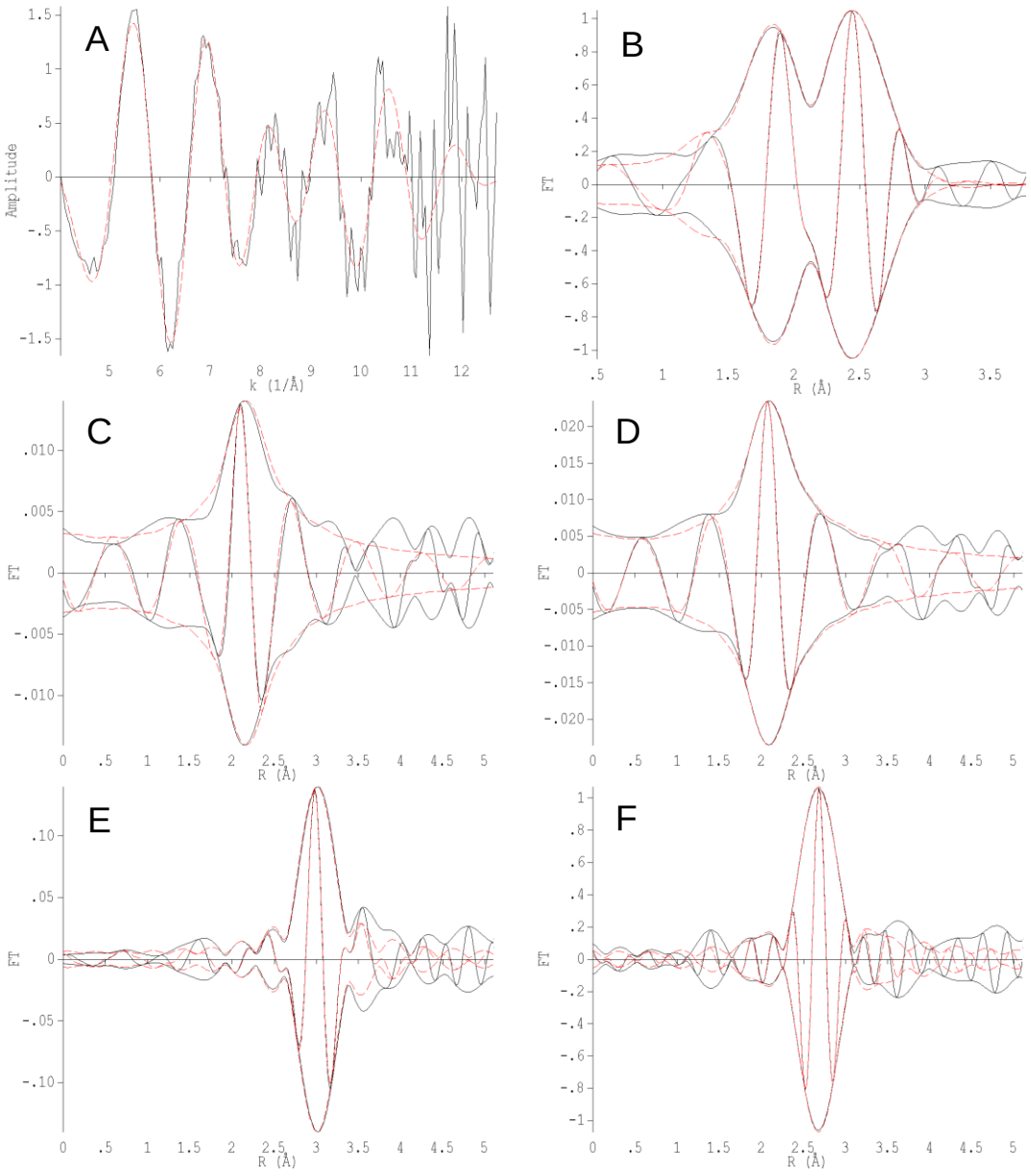

Figure S10. EXAFS data characterizing zeolite HY-supported $Ir(C_2H_4)_2$ after treatment in flowing H_2 at 300 K for 1 h: (A) k^3-weighted EXAFS function, $k^3(\chi)$ (solid line) and sum of the calculated contributions (dashed line); (B) k^3-weighted imaginary part and magnitude of the Fourier transform of the data (solid line) and sum of the calculated contributions (dashed line); (C) k^1-weighted, phase-corrected, imaginary part and magnitude of the Fourier transform of the data (solid line) and calculated contributions (dashed line) of the Ir–$O_{zeolite}$ shell; (D) k^1-weighted, phase-corrected, imaginary part and magnitude of the Fourier transform of the data (solid line) and calculated contributions (dashed line) of the Ir–C shell; (E) k^2-weighted, phase-corrected, imaginary part and magnitude of the Fourier transform of the data (solid line) and calculated contributions (dashed line) of the Ir–Al shell; (F) k^3-weighted, phase-corrected, imaginary part and magnitude of the Fourier transform of the data (solid line) and calculated contributions (dashed line) of the Ir–Ir shell.

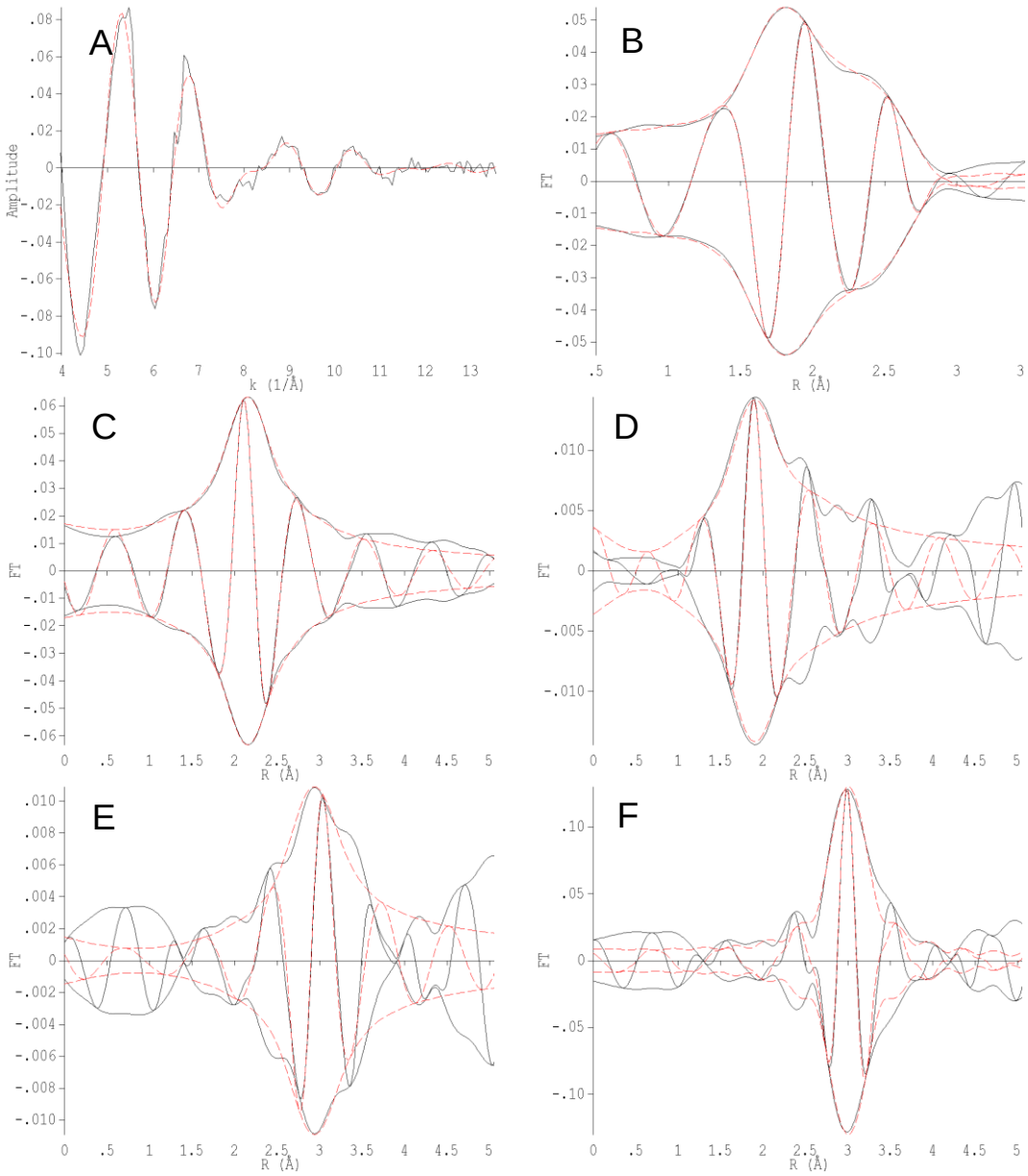

Figure S11. EXAFS data characterizing zeolite HY-supported Ir(C_2H_4)(CO) after treatment in flowing H_2 at 300 K for 1 h: (A) k^1-weighted EXAFS function, $k^1(\chi)$ (solid line) and sum of the calculated contributions (dashed line); (B) k^1-weighted imaginary part and magnitude of the Fourier transform of the data (solid line) and sum of the calculated contributions (dashed line); (C) k^1-weighted, phase-corrected, imaginary part and magnitude of the Fourier transform of the data (solid line) and calculated contributions (dashed line) of the Ir–$O_{zeolite}$ and Ir–C_{ethene} shell; (D) k^1-weighted, phase-corrected, imaginary part and magnitude of the Fourier transform of the data (solid line) and calculated contributions (dashed line) of the Ir–C_{CO} shell; (E) k^2-weighted, phase-corrected, imaginary part and magnitude of the Fourier transform of the data (solid line) and calculated contributions (dashed line) of the Ir–O_{CO} shell; (F) k^2-weighted, phase-corrected, imaginary part and magnitude of the Fourier transform of the data (solid line) and calculated contributions (dashed line) of the Ir–Al shell.

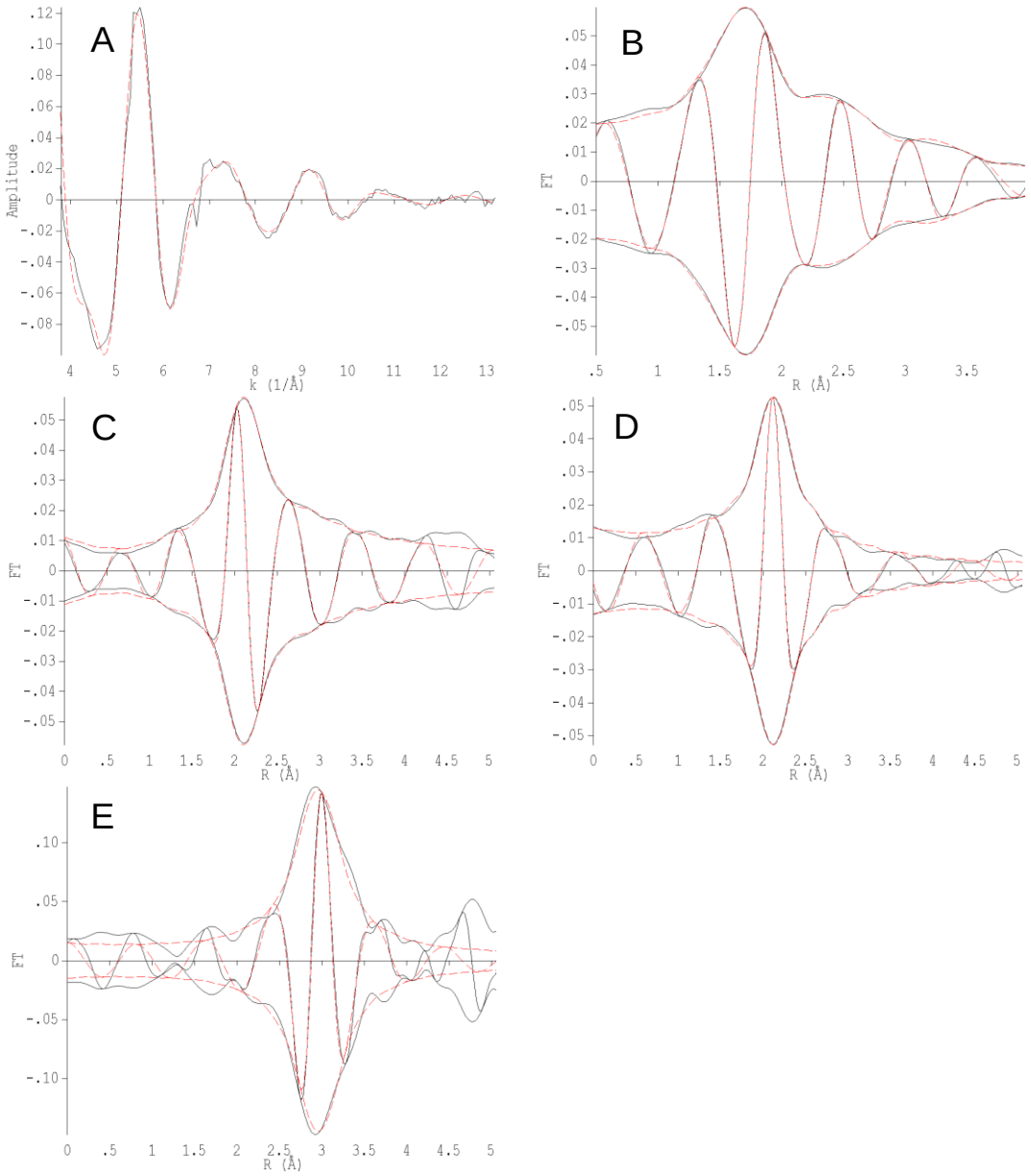

Figure S12. EXAFS data characterizing MgO-supported $Ir(C_2H_4)_2$ after treatment in flowing H_2 at 300 K for 1 h: (A) k^1-weighted EXAFS function, $k^1(\chi)$ (solid line) and sum of the calculated contributions (dashed line); (B) k^1-weighted imaginary part and magnitude of the Fourier transform of the data (solid line) and sum of the calculated contributions (dashed line); (C) k^1-weighted, phase-corrected, imaginary part and magnitude of the Fourier transform of the data (solid line) and calculated contributions (dashed line) of the $Ir–O_{zeolite}$ shell; (D) k^1-weighted, phase-corrected, imaginary part and magnitude of the Fourier transform of the data (solid line) and calculated contributions (dashed line) of the $Ir–C_{ethene}$ shell; (E) k^2-weighted, phase-corrected, imaginary part and magnitude of the Fourier transform of the data (solid line) and calculated contributions (dashed line) of the Ir–Al shell.

References

1. Bhirud, V. A.; Uzun, A.; Kletnieks, P. W.; Craciun, R.; Haw, J. M.; Dixon, D. A.; Olmstead, M. M.; Gates, B.C. *J. Organomet. Chem.* **2007**, *692*, 2107–2113.

2. Odzak, J. F.; Argo, A. M.; Lai, F. S.; Gates, B. C. *Rev. Sci. Instrum.* **2001**, *72*, 3943–3945.

3. Newville, M.; Ravel, B.; Haskel, D.; Rehr, J. J.; Stern, E. A.; Yacoby, Y. *Physica B* **1995**, *208/209*, 154–156.

4. Newville, M. *J. Synchrotron Rad.* **2001**, *8*, 96–100.

5. Vaarkamp, M.; Linders, J. C.; Koningsberger, D. C. *Physica B* **1995**, *209*, 159–160.

6. Uzun, A.; Bhirud, V. A.; Kletnieks, P. W.; Haw, J. F.; Gates, B. C. *J. Phys. Chem. C* **2007**, *111*, 15064–15073.

7. Koningsberger, D.C.; Mojet, B. L.; van Dorssen, G. E.; Ramaker, D. E. *Catal.* **2000**, *10*, 143–155.